



Remote sensing of the urban heat island effect in a highly populated urban agglomeration area in East China

Decheng Zhou ^{a,*}, Stefania Bonafoni ^b, Liangxia Zhang ^a, Ranghui Wang ^a

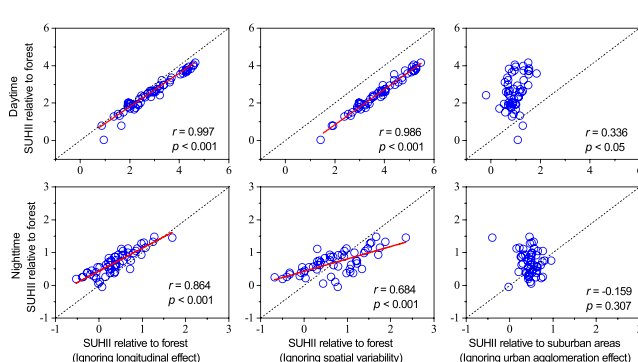
^a Jiangsu Key Laboratory of Agricultural Meteorology, Nanjing University of Information Science and Technology, Nanjing 210044, China

^b Department of Engineering, University of Perugia, via G. Duranti 93, 06125 Perugia, Italy

HIGHLIGHTS

- Surface urban heat island intensity (SUHII) was studied in an urban agglomeration.
- Four methods were used to predict the reference temperature of urban areas.
- Ignoring urban agglomeration effect would lead to large biases of SUHII estimates.
- The SUHII was evident in spite of urban size with large spatiotemporal variability.
- The climate, vegetation, surface albedo, and population density control the SUHII.

GRAPHICAL ABSTRACT



ARTICLE INFO

Article history:

Received 15 November 2017

Received in revised form 22 January 2018

Accepted 7 February 2018

Available online 13 February 2018

Editor: Ouyang Wei

Keywords:

Urbanization

City clusters

MODIS land surface temperature

Spatiotemporal trends

Driving forces

ABSTRACT

Increasingly urban agglomeration, representing a group of cities with a compact spatial organization and close economic links, can rise surface temperature in a continuous area due to decreasing distance between cities. Significant progress has been made in elucidating surface urban heat island intensity (SUHII) of a single city or a few big cities, but the SUHII's patterns remain poorly understood in urban agglomeration regions. Using Aqua/Terra MODIS data over 2010–2015, we examined the SUHII variations and their drivers in Yangtze River Delta Urban Agglomeration (YRDUA) of east China. Instead of using the widely-used suburban/rural areas as references, this study predicted the unaffected reference temperature wall-to-wall from natural forests by a simple planar surface model. Results indicated that urbanization warmed the land surface regardless of urban area size in YRDUA, with the SUHII clearly larger in the day ($2.6 \pm 0.9^\circ\text{C}$) than night ($0.7 \pm 0.4^\circ\text{C}$). The SUHII varied markedly by cities, yet the largest did not happen in the presumed core cities. Also, the SUHII differed greatly in a seasonal cycle, with summer-winter difference of $4.2 \pm 0.9^\circ\text{C}$ and $2.0 \pm 0.5^\circ\text{C}$ in the day and night, respectively. Particularly, cooling effects of urban areas were observed in winter for the majority of cities at night. These spatiotemporal patterns depend strongly on the background climate (precipitation and air temperature), vegetation activity, surface albedo, and population density, with contrast mechanisms during the day and night. Further, we showed that ignoring urban agglomeration effect (using suburban/rural areas as the unaffected references) would lead to large biases of SUHII estimates in terms of magnitude and spatial distribution. Our results emphasize the necessity of considering cities altogether when assessing the urbanization effects on climate in an urban agglomeration area.

© 2018 Elsevier B.V. All rights reserved.

* Corresponding author at: Nanjing University of Information Science and Technology, No. 219 Ningliu Road, Nanjing 210044, China.

E-mail addresses: zhoudc@nuist.edu.cn (D. Zhou), stefania.bonafoni@unipg.it (S. Bonafoni), brightzlx@126.com (L. Zhang), rhwang@nuist.edu.cn (R. Wang).

1. Introduction

The urban heat island (UHI) effect, referred to the temperature increases in urban than surrounding areas (Howard, 1833; Oke, 1973), represents one major anthropogenic modification to the Earth system in parallel with increasingly urban growth. UHI can seriously impact water and air quality (Grimm et al., 2008), local climate (Arnfield, 2003; Shepherd, 2005; Yang et al., 2017), vegetation (Zhou et al., 2014a; Zhou et al., 2016c), and energy consumption (Santamouris et al., 2015). It can also affect human health by increasing morbidity and mortality (Patz et al., 2005). These influences are expected to be more severely under a warming climate (Ward et al., 2016; Zhao et al., 2014) and a rapidly urbanizing world (Seto et al., 2012; UN, 2015). Therefore, a thorough understanding of the UHI's patterns and driving forces is critical for formulating effective mitigation and adaptation strategies.

The UHI effect has gained strong interests from scientists and urban planners in recent decades and the studies in general can be grouped into two broad types (Shepherd, 2005; Voogt and Oke, 2003). The first is the air UHI obtained from urban and rural weather stations (Huang and Lu, 2015; Oke, 1973; Peterson, 2003), which cannot provide sufficient detail for urban climate research and planning due to the limited monitoring stations (Anniballe et al., 2014; Jin and Dickinson, 2010; Wang et al., 2017). Comparatively, the second is the surface UHI calculated from remote sensing data, which has emerged as a major tool towards understanding the UHI variability owing to easy access and rich spatial coverage of satellite products (Li et al., 2017; Santamouris, 2015; Wang et al., 2017). The surface UHI intensity (SUHII), normally defined as the land surface temperature (LST) difference in urban relative to suburban or rural areas, therefore has been widely studied at local (Anniballe et al., 2014; Kong et al., 2014; Li et al., 2014, 2018; Peng et al., 2016; Wang et al., 2017; W. Zhou et al., 2017), regional (Du et al., 2016; Imhoff et al., 2010; Li et al., 2017; Santamouris, 2015; Ward et al., 2016; Zhao et al., 2014; Zhou et al., 2016a; Zhou et al., 2016b), and global (Clinton and Gong, 2013; Peng et al., 2012) scales.

Urban agglomeration (also known as city clusters), representing a group of cities having a compact spatial organization and close economic connections (Fang, 2015), has become the most salient feature of global urbanization in recent decade (Wu, 2014). It consists of at least one mega-city at the core of three or more other large cities in a specific geographical area. In contrast to individual cities, urban agglomeration can alter the thermal environment substantially in a continuous area due to decreasing or disappearing distance between cities (Du et al., 2016; Zhou et al., 2016a). However, the SUHII's patterns remained poorly understood in urban agglomerations, since most previous efforts a) focused on a single city or a few big cities, and b) assumed no UHI effect in their surrounding suburban or rural areas (Du et al., 2016; Li et al., 2017). This may not only underestimate the SUHII of the core cities (D. Zhou et al., 2015), but also fail to reveal the detailed patterns of SUHII in an urban agglomeration region. There is a clear need to better understand the UHI effects in urban agglomerations via new research protocols to help scientists and city planners make more informed decisions about the future of urban environments.

The purpose of this study was to examine the SUHII variations in Yangtze River Delta Urban Agglomeration (YRDUA) of eastern China and to explore their possible driving forces. The YRDUA is one of the most highly populated and developed regions of China and one of the six megalopolitan regions in the world (Xu et al., 2016). There are total 14 cities above the prefecture-level in YRDUA and each has a series of city-administered districts (*Shixiaqu*) and counties (*Shixiaxian*) under their jurisdiction regardless of their population size and economic strength. Numerous UHI studies have been conducted in the region, but they mainly focused on the core cities (Shanghai, Nanjing, and Hangzhou) and the city-administered districts (Kong et al., 2014; Li et al., 2011; Li et al., 2014; Li et al., 2012). A recent effort assessed the surface UHI effect in the entire YRDUA (Du et al., 2016), but they defined

suburban areas as the unaffected references that would most likely underestimate the SUHII (D. Zhou et al., 2015). These together make the YRDUA ideal for a case study of UHI effect in an urban agglomeration area. The cloud-free Landsat Operational Land Imager (OLI) images together with the latest version 6 of Moderate Resolution Imaging Spectroradiometer (MODIS) LST data were used. Unlike previous studies using loosely defined suburban/rural areas as the unaffected references (Du et al., 2016; Imhoff et al., 2010; Zhou et al., 2014b), this study estimated the reference temperature from natural forest LSTs using a simple planar surface model (Anniballe et al., 2014). The model was proved effective in predicting reference LST in a spatially-explicit manner at a regional level (Zhou et al., 2016a). We also calculated the SUHII in a traditional way in order to investigate the possible bias of SUHII estimates without considering urban agglomeration effect (assuming no UHI effect in suburban or rural areas). Finally, measurements of SUHII were correlated with a range of the background climate and urbanization factors to investigate the causes for their spatiotemporal variations.

2. Materials and methods

2.1. Study area

The boundaries of what constitutes the YRDUA vary by the perspectives of economy, culture and geography. In this study, the YRDUA (29.0–33.5° N, 118.3–122.6° E) refers to the area consisting of one core city (Shanghai), two sub-core cities (Nanjing and Hangzhou), 11 other prefecture-level cities, and 42 city-administered counties (for the convenience, the county was hereafter referred to as the city) in the southeastern part of Jiangsu Province, the northern part of Zhejiang Province, and Shanghai City, with highly diverse urbanization levels (Fig. 1). It is located in east China and has an area of about $1.03 \times 10^5 \text{ km}^2$. Most of its area is plain (with the elevation <100 m), except for the southwestern part, which is dominated by hilly lands with the maximum elevation of 1548 m. Under a typical marine monsoon subtropical climate, the mean annual precipitation and temperature in YRDUA range from 804 to 2057 mm and 9.3 to 17.3 °C, respectively. The region lies in a well-established infrastructure network containing both high-speed roads and harbor areas. In addition to the pleasant climate, the YRDUA becomes one of the most developed economic belts in China and maintains a rapid growth rate. Occupying <2.2% of China's land area, the YRDUA contributes almost a quarter of China's gross domestic product (GDP). In 2015, the GDP reached up to 10,877 billion Yuan. At the same time, the region is one of the most densely populated regions on the Earth, home to over 82.3 million people in 2015, of which approximately 53.6 million are urban dwellers. The population and GDP for each city were presented in Table 1. Evidences showed that the rapid urbanization contributed significantly to surface warming in YRDUA (Du et al., 2016; Yang et al., 2011).

2.2. Land use classification

The research team derived a 30-m land use map for year 2015 from the Landsat OLI data. The data are free to public at the U.S. Geological Survey's EROS Data Center (<http://eros.usgs.gov/>). Since cloud-free images are not available for the entire study area in 2015, eleven scenes of images spanning 2013–2016 were used in this study (Table 2). The Spectral Angle Mapper (SAM) algorithm (Kruse et al., 1993) was used to classify the land uses into five broad types including cropland, built-up land, forest, water, and unused land. The SAM method is based on the calculation of the spectral angle, which performed better than the traditional Maximum Likelihood supervised classification for multi- or hypo-spectral images (Yonezawa, 2007). The cropland refers to the lands used for crop or vegetable planting. Built-up land consists of all the impervious surfaces of cities and counties. Forest contains natural and planted forests. Water body includes reservoirs, ponds, lakes,

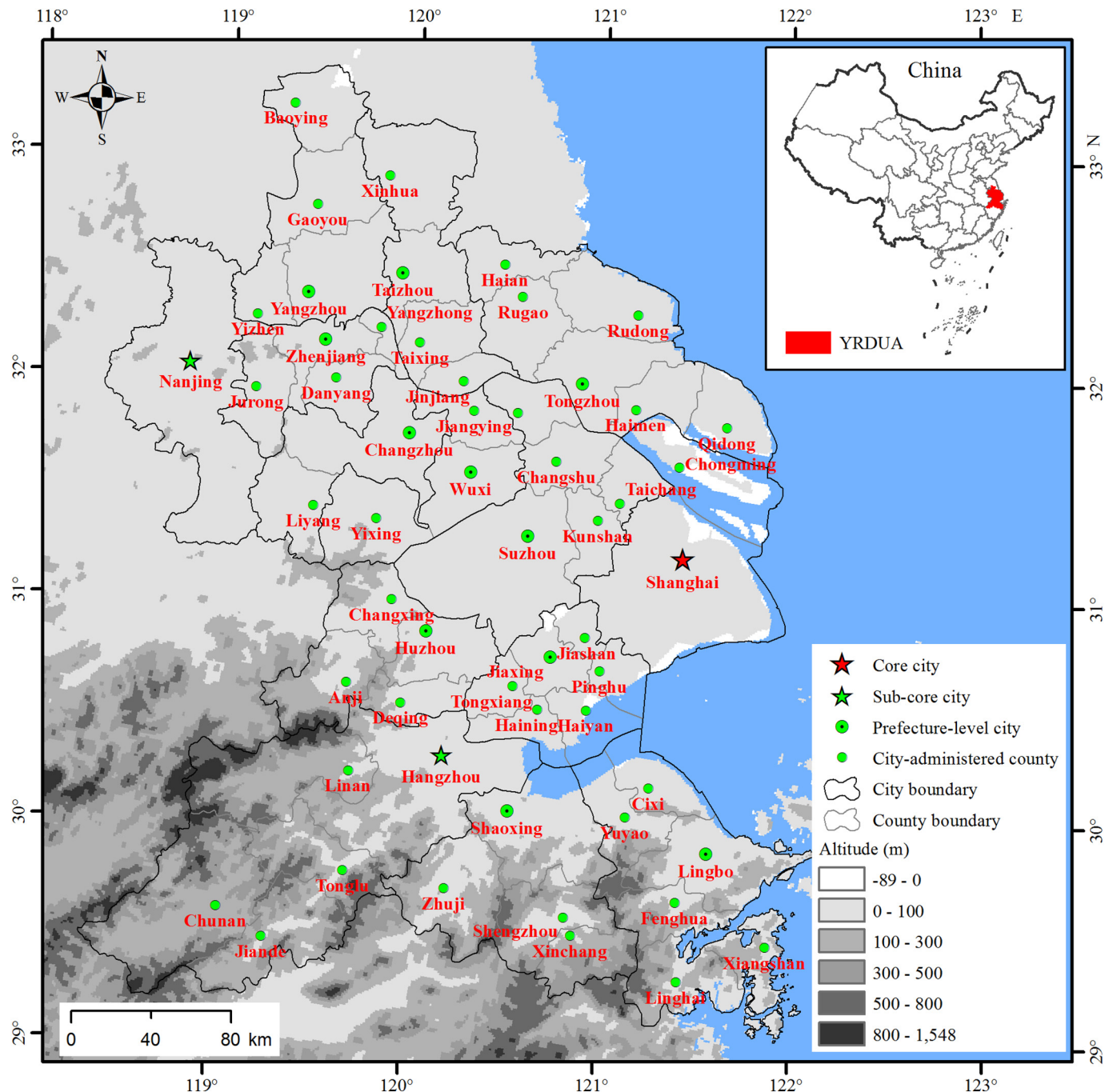


Fig. 1. Location of the 56 cities and city-administered counties in the Yangtze River Delta Urban Agglomeration (YRDUA) of China, with the background map indicating the topography.

and rivers. The unused land represents the land that is unusable or difficult to use, mainly bottomlands and mountainous rock lands with no vegetation.

The errors are unavoidable in classification due to the similarities in spectral responses of certain land covers like crop and forest lands. To reduce such errors, this study further refined the land uses by using vegetation phenology information (Zhou et al., 2016a) and global Forest/Non-Forest (FNF) map (Shimada et al., 2014). The vegetation phenology information was extracted from the 250 m Terra MODIS Enhanced Vegetation Index (EVI, 16 day composite) (MOD13Q1) in 2015. The EVI was smoothed using an adaptive Savitzky-Golay smoothing method (Chen et al., 2004) to remove the possible noise caused by atmospheric variability, cloud contamination and bidirectional effects. Phenological metrics including the maximum EVI (EVI_{max}), day of year with maximum

$EVI (DOY_{max})$, and April–June EVI difference (EVI_{dif}) were then calculated. The FNF maps (with a spatial resolution of 25 m) were provided by Japan Aerospace Exploration Agency (JAXA), which are free to download at the official website of ALOS Kyoto and Carbon Initiative. The FNF map includes three land uses (Forest, Non-Forest, and Water), with an accuracy >84%. Both MODIS and FNF images were resampled to 30 m in order to keep accordance with Landsat data.

Six splitting rules were then loosely defined according to land-use specific phenological characteristics and the FNF map (Zhou et al., 2016a): 1) change all the land into crop if $EVI_{dif} > 0$ (double growing season) and $EVI_{max} > 0.4$; 2) convert water body into cropland if $EVI_{max} > 0.4$; 3) modify urban land into forest if $EVI_{max} > 0.4$; 4) alter forest into cropland if $DOY_{max} < 144$ or $DOY_{max} > 224$ or FNF = Non-forest; and 5) convert the land into water if FNF = water.

Table 1

The total population (TP, $\times 10^4$ people), urban population (UP, $\times 10^4$ people), gross domestic production (GDP, billion Yuan), and urban area (km^2) of cities in the Yangtze River Delta Urban Agglomeration. The population and GDP data were obtained from local Statistic Yearbooks in 2014–2015. The urban areas, defined as the continuous areas dominated by high-density built-up land (>50%), were extracted from the 30 m land use map that was derived from Landsat OLI images.

City name	TP	UP	GDP	Urban area	City name	TP	UP	GDP	Urban area
Anji	46.4	13.8	28.5	11.9	Liyang	76.0	43.4	71.6	25.1
Baoying	91.1	44.7	418.3	17.0	Nanjing	823.6	670.4	972.1	637.6
Changshu	106.9	70.6	200.9	78.5	Pinghu	49.1	24.0	47.8	13.3
Changxing	63.1	16.5	43.8	11.6	Qidong	112.1	62.0	80.3	24.1
Changzhou	393.6	279.2	418.6	416.3	Rudong	104.0	56.5	67.3	15.3
Chongming	55.0	23.8	27.2	6.2	Rugao	143.6	79.4	81.2	24.2
Chun'an	45.9	8.3	19.2	2.7	Shanghai	1383.4	1275.7	2329.6	1647.3
Cixi	104.6	19.7	110.9	168.9	Shaoxing	217.8	77.3	252.8	151.4
Danyang	81.3	46.3	100.9	38.4	Shengzhou	73.3	26.0	42.3	11.5
Deqing	43.7	15.2	36.8	15.7	Suzhou	337.5	269.6	708.7	483.2
Fenghua	48.4	11.1	30.9	13.7	Taichang	47.7	31.2	106.5	64.0
Gaoyou	81.8	27.5	44.5	15.4	Taixing	119.5	68.4	73.2	18.1
Haian	94.0	52.0	68.0	33.0	Taizhou	163.6	83.8	155.5	76.4
Haimen	100.0	57.3	91.5	29.1	Tonglu	40.8	13.2	30.6	2.6
Haining	67.4	23.4	66.9	24.1	Tongxiang	68.7	27.2	61.4	24.7
Haiyan	37.8	22.1	35.1	9.6	Tongzhou	213.1	174.0	226.5	108.8
Hangzhou	525.1	358.6	797.7	217.7	Wuxi	245.7	244.2	421.7	361.0
Huzhou	110.7	49.3	86.5	25.5	Xiangshan	54.9	11.6	38.8	15.9
Jiande	51.0	13.0	29.9	3.8	Xinchang	43.9	17.2	33.4	20.2
Jiangying	123.2	55.6	275.4	177.5	Xinhua	158.2	82.1	66.6	26.0
Jiashan	38.8	18.4	40.3	15.0	Yangzhong	28.3	16.7	44.5	14.0
Jiaxing	86.4	45.9	81.8	47.0	Yangzhou	231.9	149.5	243.2	107.1
Jinjiang	66.6	41.4	70.3	31.5	Yixing	108.2	60.0	123.4	13.4
Jurong	59.1	31.8	44.1	16.8	Yizhen	56.6	26.9	46.5	23.8
Kunshan	77.0	54.8	300.1	250.3	Yuyao	83.7	19.2	80.4	62.5
Linan	53.0	11.3	43.2	14.1	Zhangjiagang	92.0	60.7	218.0	66.1
Lingbo	229.0	146.0	458.9	238.1	Zhenjiang	103.4	85.8	144.0	110.2
Linghai	62.6	10.2	41.0	15.4	Zhuji	108.0	41.0	98.1	36.3

The accuracy of the land use data was evaluated using Google Earth Pro (GE). First, a set of 500 points was sampled over the classification results of 2015. Second, these points were imported into GE and superimposed over the high-resolution images (e.g., QuickBird, IKONOS, or SPOT5) incorporated into GE. Last, the land use types of these points were compared against the images by using expert knowledge. An error matrix was created and metrics such as producer's accuracy, user's accuracy, overall accuracy, and Kappa statistics were calculated to measure the accuracy (Table 3). All land use types have relatively high accuracies except for unused land (accounting for a very small portion of the total land), with the overall accuracy and Kappa coefficient of 89.6% and 83.4%, respectively. A flowchart of this work is presented in Fig. 2.

2.3. Quantification of the surface urban heat island effect

In this study, the surface temperature was directly obtained by the latest version (version 6, 8-days composite) Aqua/Terra MODIS LST products (MYD11A2 and MOD11A2) between 2010 and 2015. The data have overpass time at 1:30, 10:30, 13:30, and 22:30 local solar hours. The MODIS LST products were estimated using a generalized

split-window algorithm under clear-sky conditions (Wan, 2014). The products have been widely validated against in-situ measurements with the bias <0.5 K in the most cases (Wan, 2014). The LST pixels with average emissivity error ≤ 0.02 (Quality control (QC) flag is '01'), average LST error ≤ 1 K (QC flag is '00'), and view zenith angle ≤ 65 degree were extracted in this analysis only.

The SUHII of an urban pixel was then defined as the temperature difference relative to forest base condition as follow:

$$\text{SUHII} (\text{x}, \text{y}, \text{z}) = \text{LST} (\text{x}, \text{y}, \text{z}) - \text{T}_{\text{forest}} (\text{x}, \text{y}, \text{z}) \quad (1)$$

where $(\text{x}, \text{y}, \text{z})$ indicates the location (longitude, latitude, altitude) of a pixel. $\text{LST} (\text{x}, \text{y}, \text{z})$ and $\text{T}_{\text{forest}} (\text{x}, \text{y}, \text{z})$ represent the actual and reference LSTs of the urban pixel, respectively. The positive SUHII means a heating effect and the opposite represents a cooling effect. The SUHII between ± 0.1 °C were assumed insignificant.

To quantify the SUHII, urban areas are needed to define and delineate on maps first. Following the convention (Schneider, 2009), this study defined urban areas as the continuous areas dominated by high-density built-up land (>50%). The urban area for each city or county was extracted from the 30 m land use map (Fig. 3a) individually

Table 2
Summary of Landsat images used in this study.

Path	Row	Acquisition date (yyyy-mm-dd)
120	38	2016-03-28
120	39	2016-03-28
119	38	2013-04-13
120	40	2015-05-12
118	38	2015-08-02
118	39	2015-08-02
118	40	2015-08-02
120	37	2014-09-30
119	37	2015-10-12
119	39	2015-10-12
119	40	2015-10-12

Classified	Reference					Total	User
	Cropland	Built-up land	Forest	Water	Unused land		
Cropland	250	5	10	3	0	268	93.3
Built-up land	11	74	2	0	2	89	83.1
Forest	13	1	90	0	0	104	86.5
Water	3	0	0	31	0	34	91.2
Unused land	1	1	0	0	3	5	60.0
Total	278	81	102	34	5	Overall = 89.6	
Producer	89.9	91.4	88.2	91.2	60.0	Kappa = 83.4	

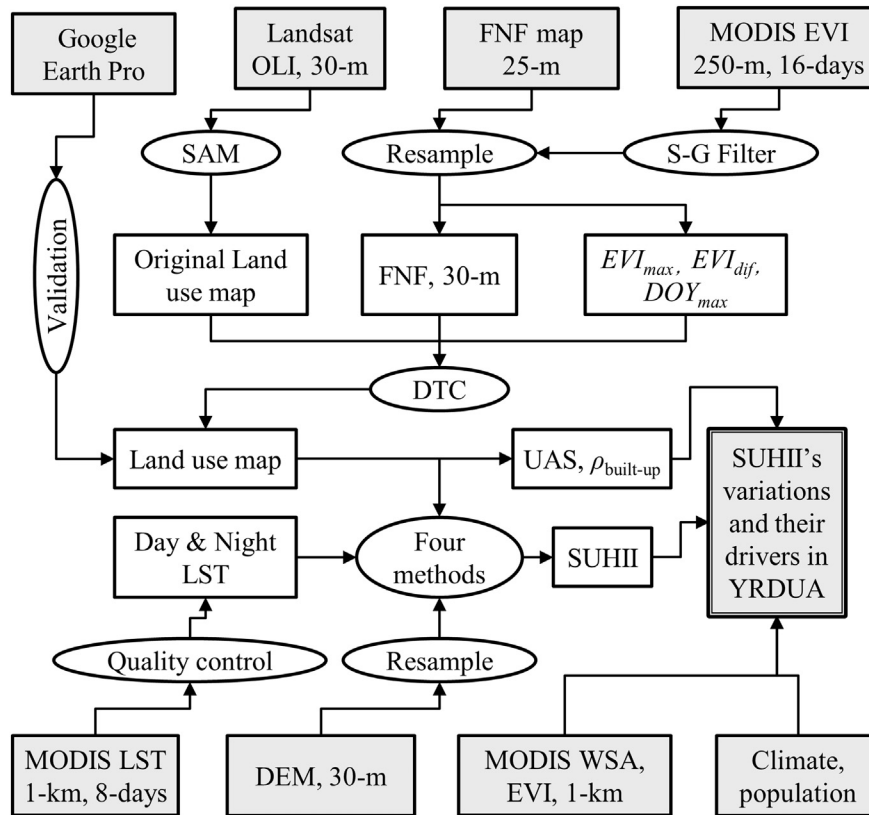


Fig. 2. Research flowchart for examining the surface urban heat island intensity (SUHII) in YRDUA. SAM, Spectral Angle Mapper supervised classification; DTC, Decision Tree Classification; S-G, Savitzky-Golay; FNF, Forest/Non-Forest; EVI, Enhanced Vegetation Index; LST, Land Surface Temperature; EVI_{\max} , maximum EVI; DOY_{\max} , day of year with maximum EVI; EVI_{dif} , April-June EVI difference; WSA, White Sky Albedo; $\rho_{\text{built-up}}$, built-up intensity; UAS, Urban Area Size;

through a moving window method proposed by Zhou et al. (2014b). Urban pixels less than two kilometers away from the perimeter of water body were excluded, because their UHI effects may have been overshadowed by the cooling (in the day) or warming (at night) effects of nearby water body (Imhoff et al., 2010; D. Zhou et al., 2015). The resultant urban areas in 2015 ranged from 2.6 km² in Tonglu county to 1646.3 km² in Shanghai city (Fig. 3b).

The reference temperature, $T_{\text{forest}}(x,y,z)$, was then estimated from natural forest LSTs wall-to-wall by a simple planar surface model (Anniballe et al., 2014; Zhou et al., 2016a) in order to reduce the impacts of topography and geographic locations as follow (referred as method 1):

$$T_{\text{forest}}(x,y,z) = T_0 + a_1 x + a_2 y + a_3 z \quad (2)$$

where $T_{\text{forest}}(x,y,z)$ represents the reference LST at (x,y,z) , T_0 is a constant, a_1 , a_2 , and a_3 are the coefficients describing the spatial gradient of forest temperature. These coefficients are critical for an accurate estimation of the SUHII. We determined them by the following steps:

- 1) Forest lands were subset from the land use map and aggregated to a spatial resolution of 1 km² in order to match the LST data. The forest pixels located in the 50 km buffer zones of the YRDUA were also included in order to increase the natural forest coverage.
- 2) The forest distributed in the 2 km buffer zones of urban lands and water bodies were masked out because their LSTs might be impacted by nearby urban and/or water land uses.
- 3) The remaining forest pixels were superimposed over the high-resolution images in Google Earth Pro to exclude the miss-classified pixels and urban green spaces. About 19,904 natural forest pixels were selected eventually by the combination use of expert knowledge (Fig. 3b).

- 4) Multiple linear regression analysis between forest LSTs and their 3-D location parameters (x, y, z) was performed to determine the T_0 , a_1 , a_2 , and a_3 values for each image using a number of valid LST values (after the data quality control) larger than 10,000. The elevation data was obtained from the Advanced Spaceborne Thermal Emission and Reflection Radiometer Global Digital Elevation Model (ASTER GDEM) (Tachikawa et al., 2011) (Fig. 1). The forest LSTs were closely related to their location parameters, with mean coefficient of determination r^2 of 0.39 ± 0.13 and 0.35 ± 0.15 for the day and night, respectively.

The annual, monthly, and seasonal (summer and winter) SUHII in the day (average of the SUHII at 10:30 and 13:30) and night (average of the SUHII at 1:30 and 22:30) were calculated for each city and each year separately. Summer and winter refer to the periods of June to August and December to February, respectively. Due to climate variability, urban development, and/or varying data quality, the SUHII estimates may vary greatly by year. Therefore, the SUHII were averaged over the period 2010–2015 at last in order to obtain an overall pattern for each city.

To examine the sensitivity of SUHII estimates to the inferring method of reference LST from natural forests, this paper estimated the SUHII using two other methods (referred to method 2 and method 3). Method 2 defined the reference LST as a function of latitude and altitude. The longitudinal variations were not considered in order to avoid the possible effect of land sea breeze. Method 3 ignored all the spatial variability and used the mean LST of all natural forest pixels as the reference for all the cities.

The reference LSTs (T_{forest}) estimated using method 1 (considers variations in latitude, longitude, and altitude) and method 2 (did not consider the longitudinal effects) were presented in Fig. 4. The predicted T_{forest} overall decreased with rising elevation and latitude (Fig. 4a and b), agreeing well with the general temperature patterns across the

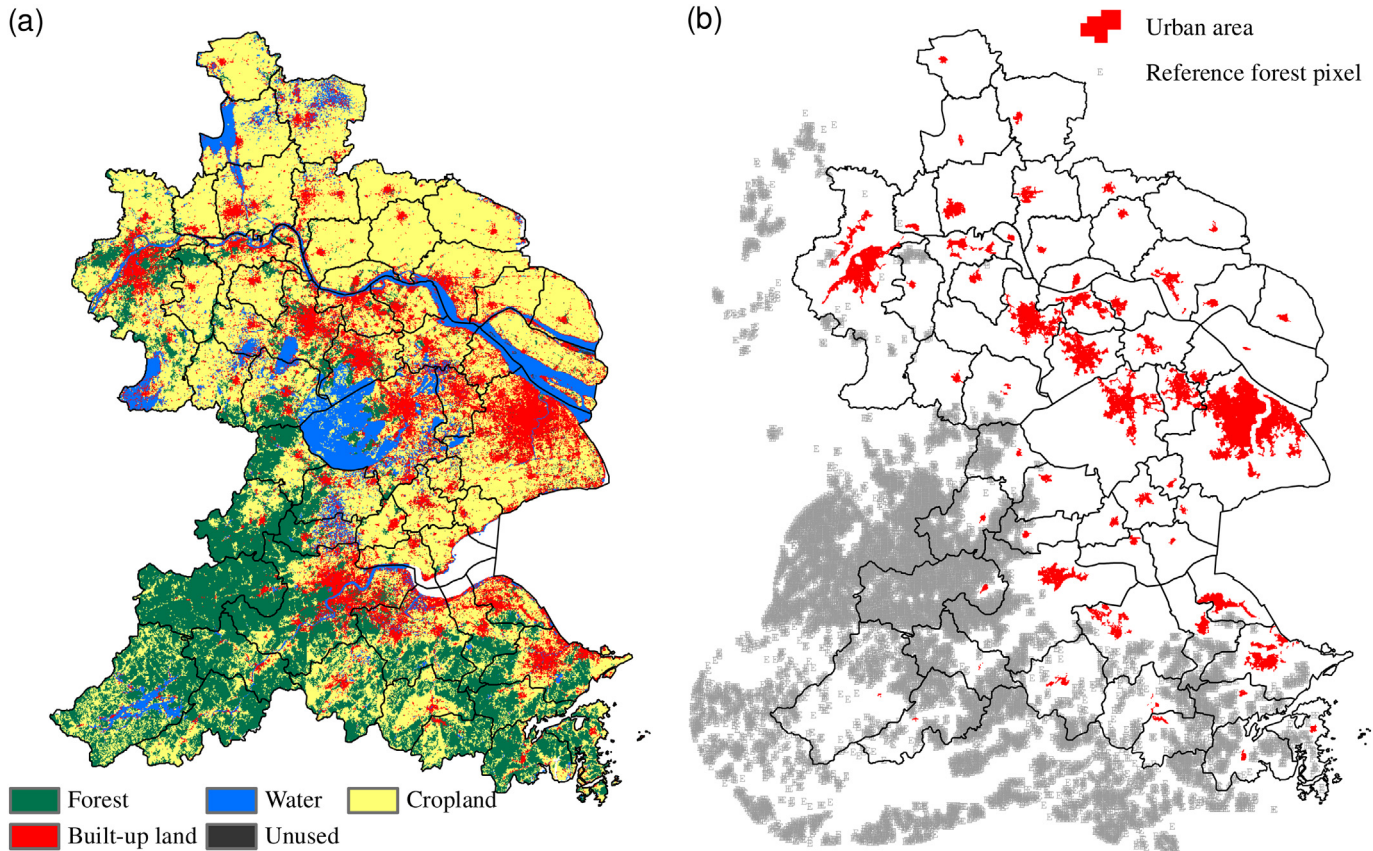


Fig. 3. The 30 m land use map in circa 2015 derived from Landsat Operational Land Imager (OLI) images (a), and the urban area and reference forest pixels derived from the land use map (b).

globe. The T_{forest} estimated using method 2 was highly consistent with that by method 1 during the daytime (Fig. 4a and c). By contrast, the nighttime T_{forest} were underestimated by method 2 in the southern part of YRDUA, indicating possible influence of land sea breeze on forest LST, especially at night.

For a comparison analysis, we also estimated SUHII in a traditional manner as urban-suburban/rural LST differences (Du et al., 2016; Imhoff et al., 2010; Peng et al., 2012; Zhou et al., 2014b). The lands 25–30 km away from urban areas that outside the UHI footprint were defined as the rural areas (Imhoff et al., 2010; D. Zhou et al., 2015). The buffer zone surrounding urban area that has the same size as urban area were defined as the suburban areas (Peng et al., 2012; Zhou et al., 2014b). Built-up lands, water body, and buffer areas overlapped by two or more cities were excluded. Lands close to water body (<2 km away from water border) or at an elevation 50 m higher than the highest urban pixel were also removed from the reference areas. Since no rural pixels left in most cities after these excluding actions (Fig. 5), this study calculated urban-suburban LST differences only (referred to method 4).

2.4. Exploring the possible drivers of surface urban heat island effect

Datasets related to both the background climate and urbanization were assembled to explore the possible causes for the SUHII's variations. The average monthly climate data (1970–2000) of precipitation, air temperature, solar radiation, and wind speed (with a spatial resolution of approximately 1 km²) were obtained from WorldClim 2.0 (Fick and Hijmans, 2017). Although they may differ from the actual climate during the study period (2010–2015) due to climate variability, their spatial and seasonal patterns should not change significantly through the time. Urbanization factors including the differences of urban EVI and surface albedo relative to forest base conditions, built-up intensity ($\rho_{\text{built-up}}$), population density (ρ_{popu}), and urban area size (UAS) were

considered in this analysis. The $\rho_{\text{built-up}}$ was defined as the urban area percentage per each LST pixel. The EVI data from 2010 to 2015 were obtained from 1-km MODIS EVI products (MOD13A2, 16-day composites). The white sky albedo (WSA, bi-hemispherical reflectance) was extracted from MODIS albedo products (MCD43C3, 8-day composites). WSA with best (QC = 0), good (QC = 1), or mixed (QC = 3) quality are used only. The differences of EVI and WSA (ΔEVI and ΔWSA) between urban and natural forest lands were calculated by the same method as method 1 for the SUHII. The ΔEVI and ΔWSA were then aggregated to a monthly level. The $\rho_{\text{built-up}}$ and UAS for year 2015 were extracted from the land use map directly. The ρ_{popu} of each city was obtained from the Gridded Population of the World Version 4 (GPWv4) (CIESIN, 2016). This data set is based on the data from the United Nations World Population Prospects 2015 Revision (UN, 2015), with a spatial resolution of 30 arc-seconds. The $\rho_{\text{built-up}}$, UAS, and ρ_{popu} were assumed constant through a year, since there was no seasonal information of them.

The Pearson's correlation coefficients (r) between such variables and SUHII across cities were estimated at monthly and annual mean scales. Stepwise linear regressions were developed to find the independent explanation rate of each selected variable (represented by the R-squared change) and the total explanation rate (the total R-squared of the model) of those potential driving variables to the spatial variation of SUHII. In addition, the r between SUHII and those variables (with seasonal information available) across months were computed for each urban pixel, individually.

3. Results

3.1. Spatial patterns of SUHII

The SUHII estimated by method 1 is primarily used in this analysis. Fig. 6 shows the spatial distribution of the SUHII (i.e., the mean SUHII

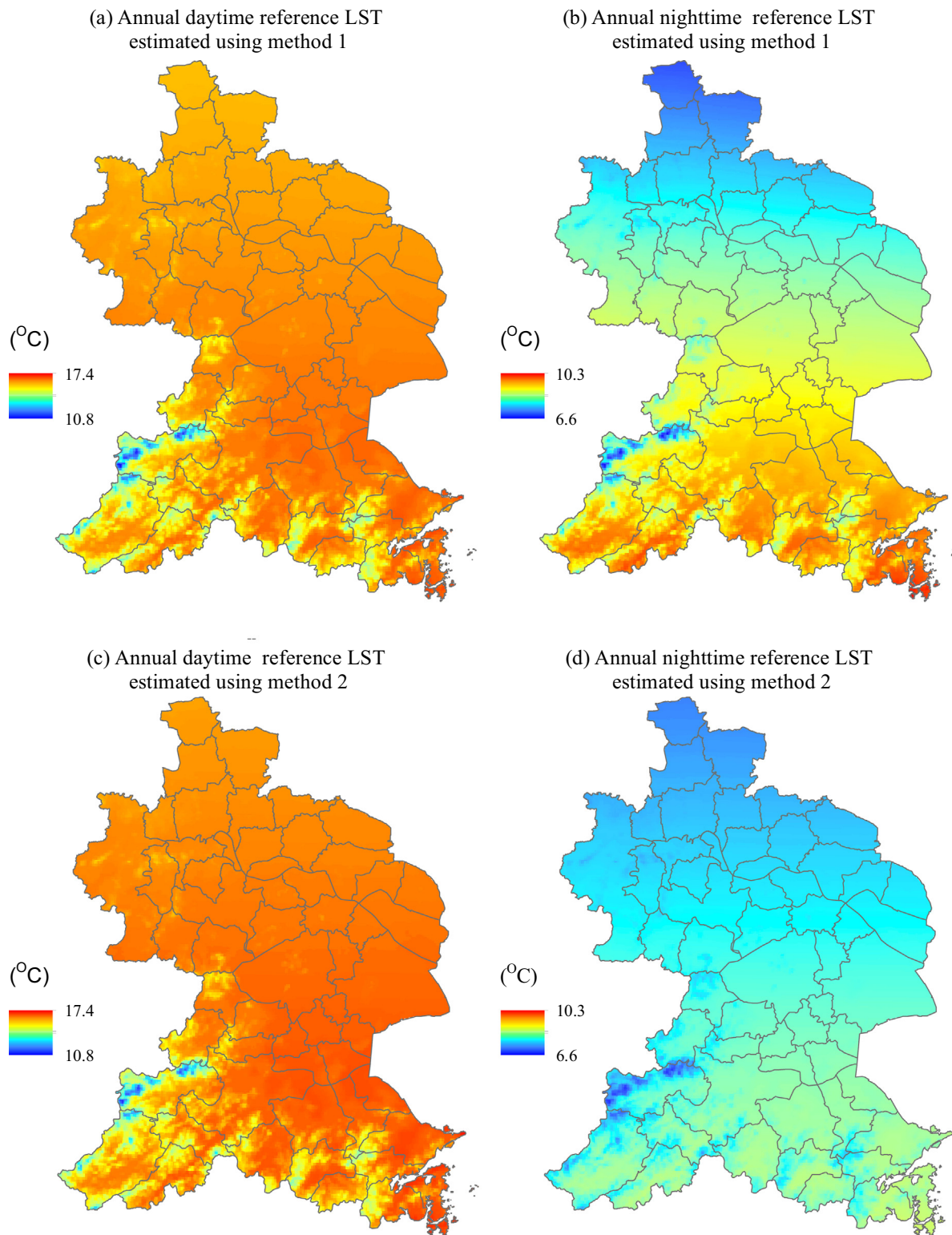


Fig. 4. Spatial distribution of the annual mean (2010–2015) reference LST estimated by method 1 (function of longitude, latitude, and altitude) and method 2 (function of latitude and altitude).

of all urban pixels for each city) averaged over the period 2010–2015 for the 56 cities in the YRDUA. The annual mean daytime SUHII were positive in all those cities varying from 0.17 °C in Chun'an county to 4.19 °C in Yuyao city (Fig. 6a). Cities located in southeastern part of YRDUA experienced more intense SUHII during the day than those in the North. The annual mean night SUHII were also positive in all the cities but two counties (Tonglu and Anji) where insignificant effects being

observed (Fig. 6e). The cities in the central-east part overall showed more evident warming effect than the southern and northern counterparts. The SUHII was clearly larger in the day than night, especially in southeastern YRDUA, as indicated by positive day-night differences (DNDs) for nearly all those 56 cities (Fig. 6i). On average, the annual mean SUHII was 2.7 times higher in the day (2.6 ± 0.9 °C) than night (0.7 ± 0.4 °C) in YRDUA.

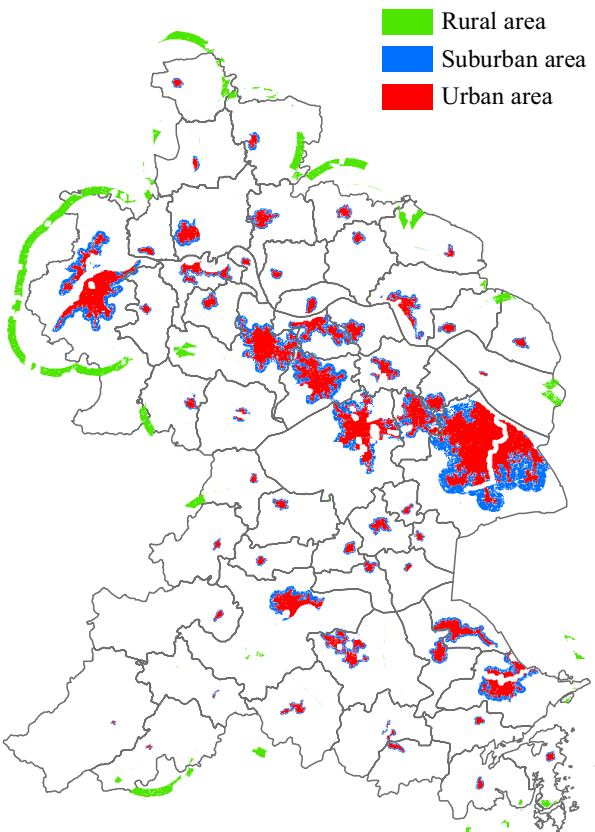


Fig. 5. Spatial distribution of the loosely defined unaffected suburban/rural areas. Built-up lands, the lands >50 m higher than the highest urban pixel, water body, and the lands near water body were excluded. The reference areas overlapped by two or more cities were also excluded.

The SUHII differed greatly in a seasonal cycle. During the daytime, the SUHII was significantly higher in summer ($4.7 \pm 1.2^\circ\text{C}$) than in winter ($0.5 \pm 0.8^\circ\text{C}$) for all the cities, with the mean summer-winter difference (SWD) of $4.2 \pm 0.9^\circ\text{C}$ (Fig. 6d). The same trend happened at night, but with a much smaller SWD of $2.0 \pm 0.5^\circ\text{C}$ (Fig. 6h). In particular, cooling or insignificant effects of urban areas relative to natural forest base conditions have been observed in 20 out of 56 cities (mostly distributed in the north part of YRDUA) in the winter season during the daytime (Fig. 6c). Comparatively, nearly all the cities demonstrated a cooling effect in the winter season at night (Fig. 6g). More specifically, the SUHII were the strongest in July and the weakest in January during both the day and night time periods (Fig. 7). Interestingly, the nighttime SUHII dropped dramatically in June, followed by a sharp increase in July. The diurnal cycle of SUHII also varied substantially by season, with overall DNDs of $3.3 \pm 1.1^\circ\text{C}$ and $0.8 \pm 0.9^\circ\text{C}$ in the summer and winter, respectively (Fig. 6j and k). Spatially, the daytime SUHII related positively and significantly with nighttime SUHII across the 56 cities in summer ($r = 0.44$, $p < 0.01$). In contrast, no correlation was shown between them in winter ($p = 0.11$) (Fig. 8). Meanwhile, a statistically significant correlation was illustrated between summer and winter SUHII in both the day and night ($p < 0.01$).

Fig. 9 shows the correlations between annual mean SUHII across cities estimated by the four methods as described in Section 2.3. As can be seen, the SUHII estimated by method 1 (used in current analysis) agreed well with that from method 2, in particular during the day (Fig. 9a and b). This indicates a small influence of land sea breeze on SUHII estimates. Method 3 overestimated the SUHII in the day and over- or under-estimated the SUHII at night substantially, though their spatial patterns were highly consistent (Fig. 9c and d). The SUHII estimated by method 4 that defines SUHII as temperature difference between urban and suburban areas were completely different from that

by the first method in terms of magnitudes and spatial patterns (Fig. 9e and f). For example, method 4 on average underestimated the SUHII by 63% in the day and by 38% at night as compared with method 1. In addition, a weak ($r = 0.34$, $p < 0.05$) and a statistically insignificant ($p = 0.31$) correlation between those two SUHII estimates were observed for the day and night, respectively.

3.2. Relationships between SUHII and the background climate or urbanization factors

To explore the potential drivers of the SUHII's spatial patterns, Fig. 10 demonstrates the Pearson's correlation coefficients (r) between SUHII and nine variables across the 56 cities on both annual mean and monthly scales. During the daytime, the spatial variations of SUHII were closely and negatively correlated with ΔEVI and solar radiation, and positively linked to background precipitation or air temperature (Fig. 10a). Urban area size and population density contributed positively to SUHII's spatial variability, but the correlations were overall not statistically significant. During the night, the SUHII correlated more closely and negatively to ΔWSA and ΔEVI , and positively to population density. The climatic factors (precipitation, temperature, and solar radiation) also impacted the nighttime SUHII, with reverse correlations being observed in different months. Interestingly, a weak negative correlation between SUHII and built-up intensity was observed in YRDUA regardless of the time periods. Meanwhile, the SUHII correlated positively and significantly with wind speed across space in approximately half a year.

Stepwise linear regression analysis indicated that the factors compiled in this paper (Fig. 10a) explained a greater portion of SUHII variation (represented by the total R-square of the linear model) in the day compared to night (82% versus 57%) on an annual mean scale (Fig. 10b, last row). The explanation rates of those factors varied greatly by month, with the largest in January and the lowest in June in both the day and night. The daytime SUHII was primarily explained by solar radiation, temperature, and precipitation. In contrast, the population density, ΔWSA , and precipitation accounted for most SUHII's variations at night.

Intra-annually, the SUHII variations across months were tightly and positively correlated with the background climate factors of air temperature, solar radiation, and precipitation, and negatively with ΔEVI for the majority of 56 cities, with the mean r larger than 0.81 and 0.57 for the day and night, respectively (Fig. 11). The ΔWSA and wind speed in general contributed little and negatively to the SUHII's seasonality.

4. Discussion

As expected, our results showed that ignoring urban agglomeration effect (i.e., using loosely defined rural or suburban areas as affected reference) not only underestimated the SUHII substantially, but also resulted in large bias in the SUHII's distribution. For example, the annual mean daytime SUHII estimated in this study was 2.7 times that estimated by urban-suburban temperature difference (Fig. 9e and f). The underestimation can be also seen clearly by comparing our results with that from one recent study by Du et al. (2016). They found that the SUHII defined as the temperature difference between urban and suburban areas was 0.8°C in YRDUA in summer, which was far lower than the 4.6°C estimated in this study. Our method is more reasonable for three reasons. First, the distance between urban areas tends to decrease and even disappear with accelerating urban land expansion (Fang, 2015), ultimately leading to the loss of un-affected lands in the presumed suburban and rural areas. This was especially true for the metropolitan areas of Shanghai, Suzhou, and Wuxi in YRDUA (Fig. 3a). Second, the UHI effect usually can transcend far from its physical boundary (D. Zhou et al., 2015), suggesting that temperature in suburban areas will be affected by the UHI effect to a certain extent by nature. Finally, the suburban/rural areas, even though not being urbanized, are mostly covered by cropland, the thermal conditions of which depend

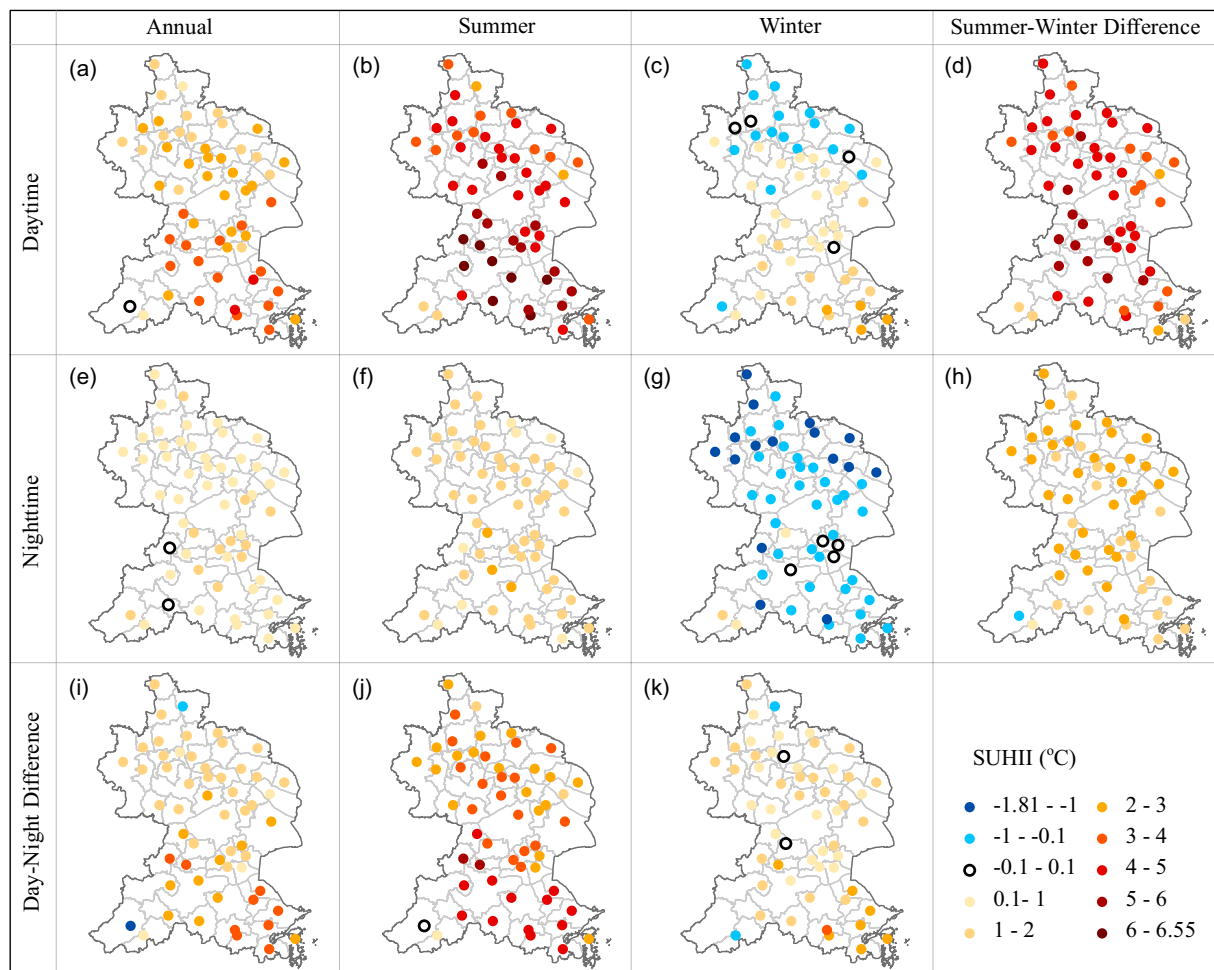


Fig. 6. Spatial patterns of SUHII averaged over the period 2010–2015 in YRDUA, including annual mean estimates, and their seasonal counterparts.

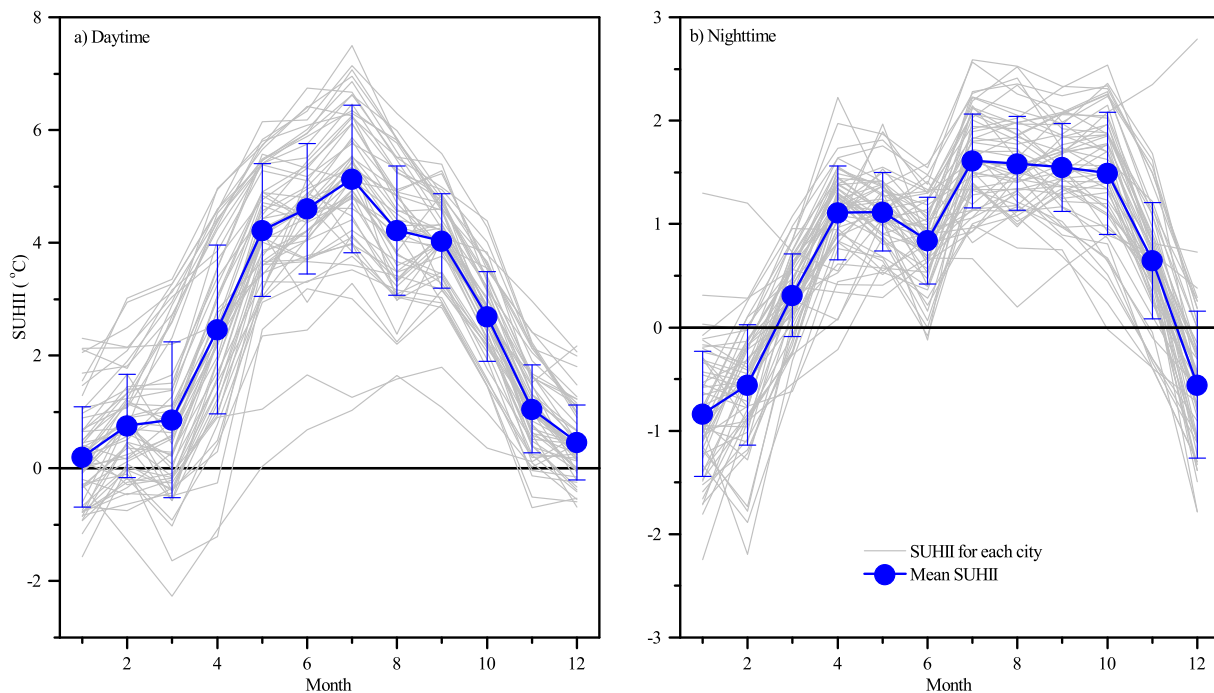


Fig. 7. Intra-annual variations of SUHII averaged over the period 2010–2015 in YRDUA. The error bar represents one standard deviation across cities.

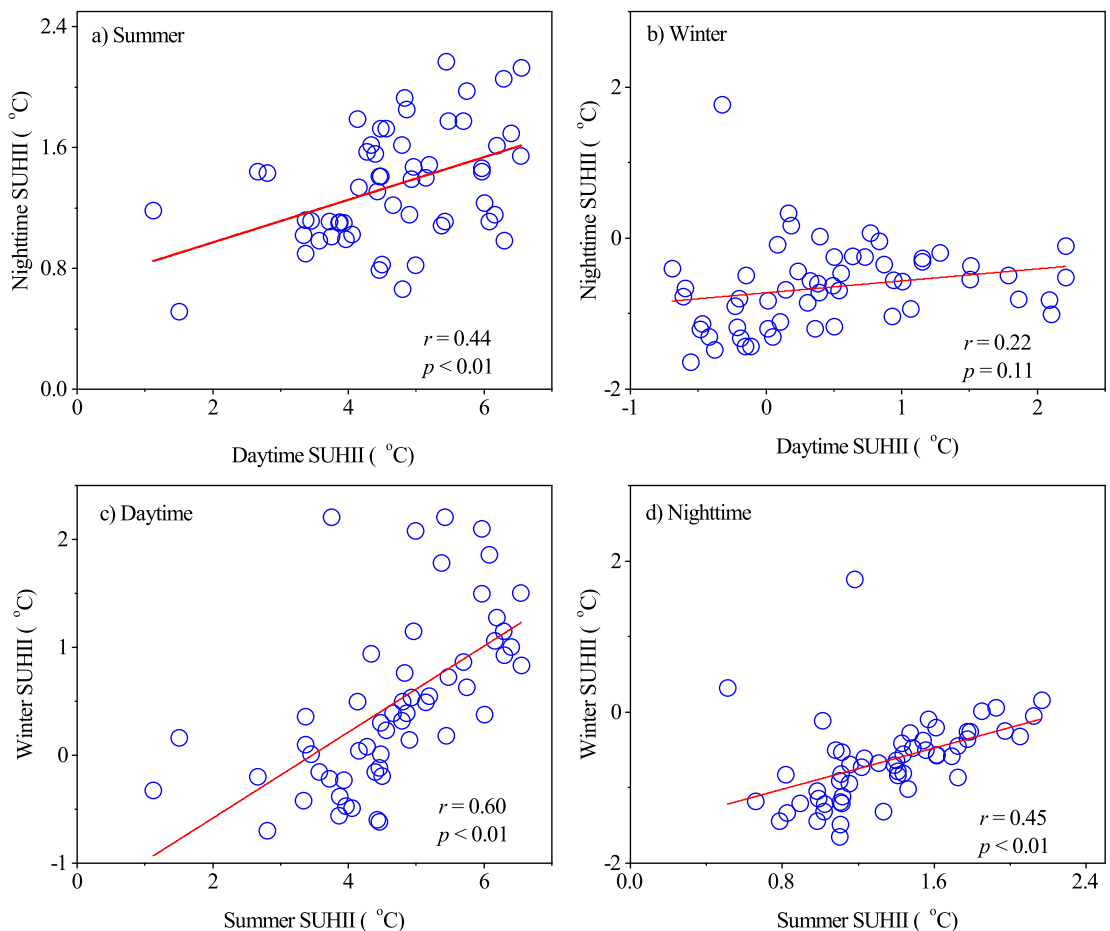


Fig. 8. Correlations between day and night SUHII (a, b) and between summer and winter SUHII (c, d) across cities ($N = 56$).

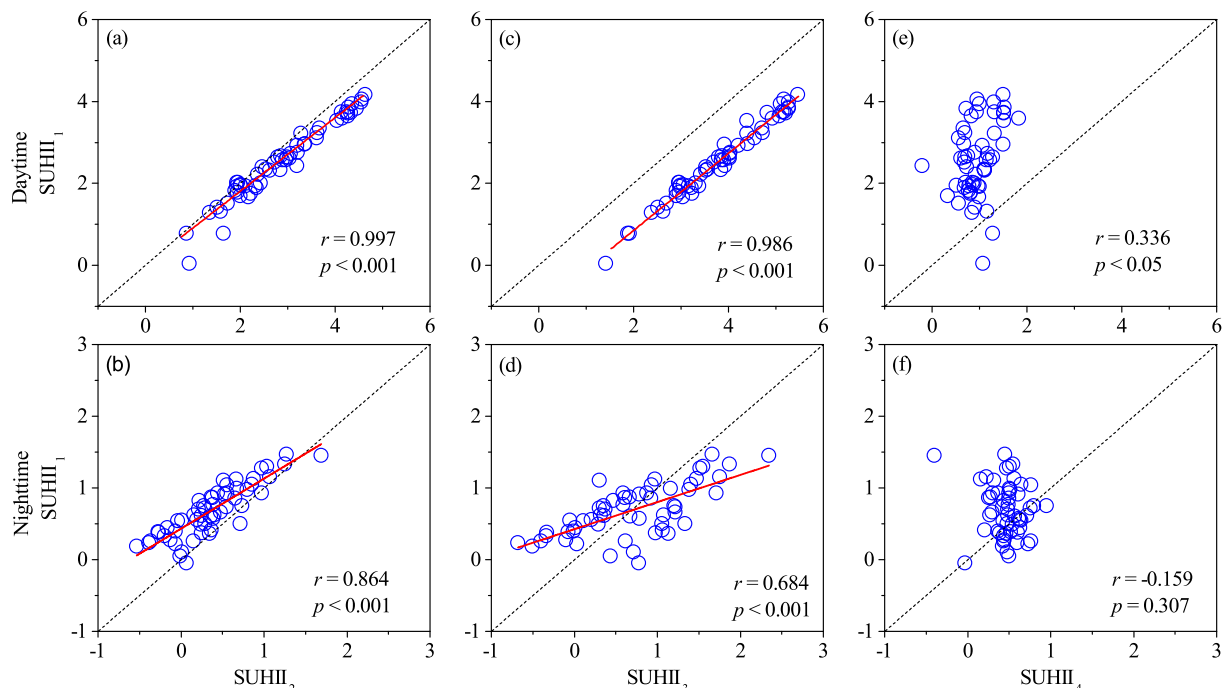


Fig. 9. Comparison of annual mean SUHII with the reference temperatures estimated by the four different methods (indicated by the subscript) ($N = 56$).

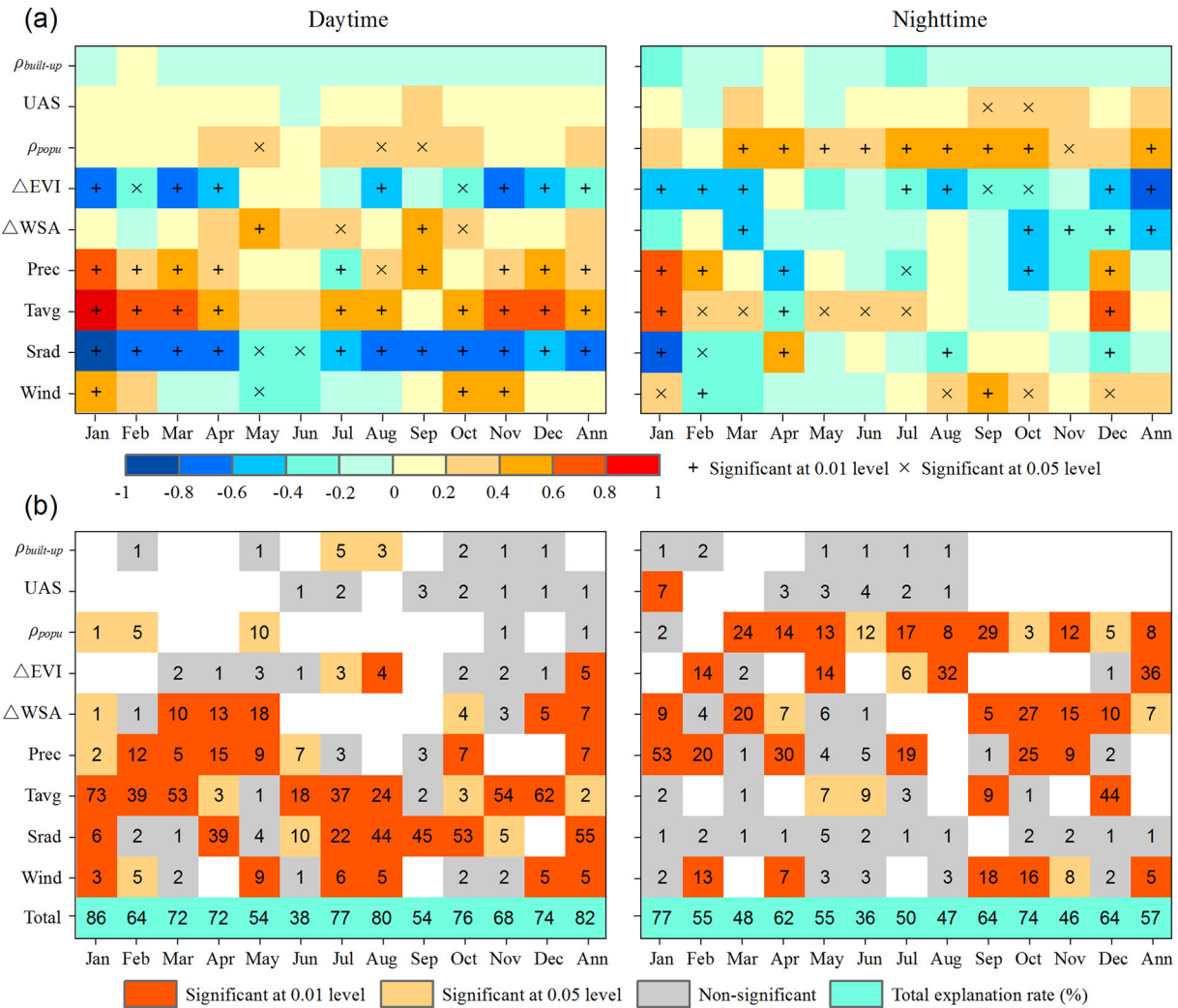


Fig. 10. Relationships between the SUHII and driving variables across cities ($N = 56$) on monthly and annual mean scales as indicated by the Pearson's correlation coefficients (r) in YRDUA (a), and the independent (R-squared change) together with the total (total R-squared of the model) explanation rates of those driving variables on the SUHII's variations (%) derived from stepwise linear regression analysis (b). The white grid in panel b indicates no independent contribution to the SUHII's variability. ρ_{popu} , population density; Prec, precipitation; Tavg, mean air temperature; Srad, solar radiation; Wind, wind speed. Δ , difference relative to forest base condition.

strongly on site-specific agricultural activities (in particular the cropping system and irrigation practice) (Zhou et al., 2016a). Comparatively, lands covered by natural vegetation (e.g., forests in present study

area) can be served as the best and perhaps the only unaffected reference for estimating SUHII in such highly developed urban agglomeration regions.

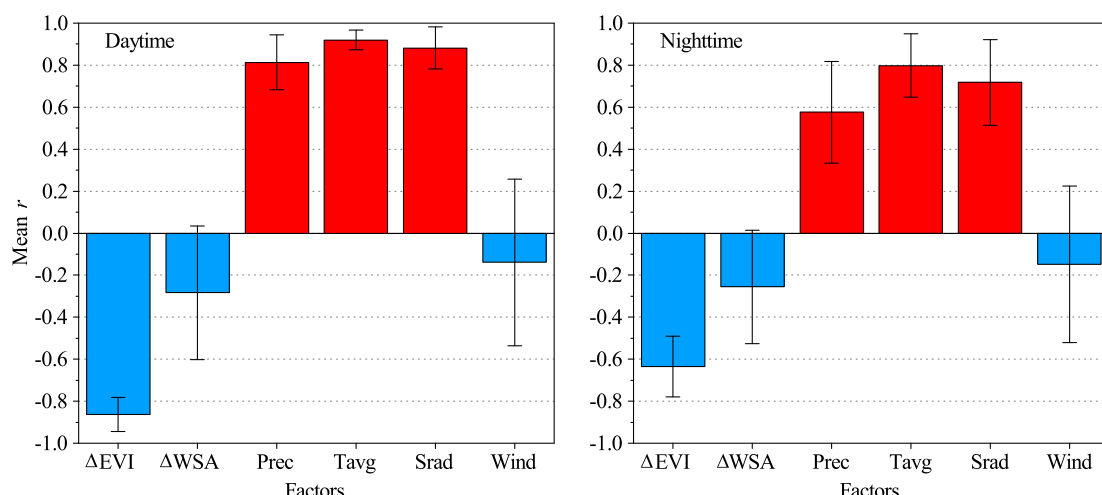


Fig. 11. The r between the SUHII and driving factors across months ($N = 12$) averaged over the 56 cities in YRDUA. The error bar represents one standard deviation across cities.

4.1. Spatial variability of SUHII in YRDUA and their drivers

Similar to previous findings in various spatial scales (Du et al., 2016; Imhoff et al., 2010; Li et al., 2011; Peng et al., 2012; Zhou et al., 2014b), our results indicated that urbanization warmed the land surface temperature on an annual mean scale regardless of urban area size, with the SUHII clearly larger during the day compared to that at night (Fig. 6). The stronger daytime SUHII can be attributed to the substantial reduction of latent heat flux caused by the decrease of vegetation activity associated with urbanization in humid-hot region (Hao et al., 2015). Meanwhile, high soil moisture content and small surface albedo of humid forests (Hall, 2004) can help store heat during the day, ultimately leading to the relatively small LST contrast between urban areas and forests at night (Peng et al., 2012; Zhou et al., 2014b).

The SUHII varied dramatically by cities that depend strongly on both the background climate and urbanization factors (Figs. 6 and 10). In general, the weak correlations between day and night SUHII (Fig. 8a and b) confirmed the different underlying mechanisms between day and night (Oke, 1982). Specifically, the daytime SUHII related closely and positively to the background precipitation or air temperature across cities in YRDUA (Fig. 10), agreeing well with previous findings in North America (Imhoff et al., 2010; Zhao et al., 2014) and China (Zhou et al., 2016b). The wetter cities typically have larger soil moisture content under natural conditions, which help reduce the heating rate of forest land during the day, consequently leading to higher SUHII (Oke, 1982). At the same time, increase in ambient temperature can intensify the UHI effect by shifting the incoming radiative energy partitioning in favor of more latent heat flux (evapotranspiration) and ground heat flux, and reducing the wind speed (Li and Bou-Zeid, 2013). Moreover, other variables associated with surface UHI effect, such as surface albedo (Hall, 2004), vegetation activity (Zhou et al., 2014a), and anthropogenic heat emissions (Santamouris and Asimakopoulos, 2001) were strongly controlled by the background climate. For instance, urbanization in hot-wetter region usually leads to a greater decrease of vegetation activity, accompanied by a higher SUHII (Li et al., 2011; Peng et al., 2012). This can be verified by the significant negative correlations between daytime SUHII and ΔEVI in this study (Fig. 10a).

Comparatively, the nighttime SUHII related tightly and positively to population density, and negatively to ΔWSA and ΔEVI (Fig. 10). Urban area with larger population density normally has more buildings, pavements, and energy consumption, and thus has more energy for releasing at night (Du et al., 2016). In contrast, urban area with larger surface albedo were expected to have lower heat storage (Arnfield, 2003; Oke,

1982; Shepherd, 2005), ultimately leading to smaller nighttime SUHII. The negative relationship between ΔEVI and nighttime SUHII can be also explained in terms of heat storage. For example, reduction of vegetation activity in urban areas could raise the ground heat flux in parallel with the increase of sensible heat flux, therefore exaggerating the SUHII at night (Zhou et al., 2016a).

Urban area size contributed positively to SUHII in both the day and night, though the correlations were not statistically significant in most months (Fig. 10a). Impacts of urban area size on SUHII were complicated and can be attributed to multiple reasons (Li et al., 2017; B. Zhou et al., 2017). First, the building height tends to be higher in larger urban areas, which can help absorb and store more heat, consequently leading to higher SUHII at night. Second, vegetation activity usually decreases with urban development (Zhou et al., 2014a), and thus cooling effect of urban greenspace may be weaker in larger cities than that in smaller counterparts. Third, population density and economic activities (e.g. transportation) are usually higher in larger urban areas, resulting in greater amount of anthropogenic heat releases (Clinton and Gong, 2013; B. Zhou et al., 2017).

Exceptional results were also observed in this study. Solar radiation, supposedly contributing positively to temperature, was negatively linked to daytime SUHII in YRDUA (Fig. 10). This is possibly due to the multicollinearity problems among different factors. For instance, humid-hot cities with strong SUHII normally have more clouds and more severe air pollution, both can decrease incoming solar radiation through absorption and reflection. This can be verified by strong negative correlations between solar radiation and air temperature or precipitation (Fig. 12). Additionally, wind speed (presumably reduce SUHII through accelerating temperature exchange between urban and surrounding areas) and built-up intensity (normally can intensify SUHII by increasing heat storage and anthropogenic heat releases) were found to be weakly related to SUHII. This was most likely due to small variations of them among cities that were not enough to cause significant impacts.

Overall, we found that the factors integrated in current research explained a greater portion of the SUHII's variability in the day than night (Fig. 10b, last row), suggesting possible more complicated mechanisms underlying SUHII at night. This finding was consistent with that by Peng et al. (2012) at a global scale, but was contrary to our previous results at a national scale in China (Zhou et al., 2014b). The disparity can be attributed partially to the contrast SUHII estimation methods between this and previous studies and partially to the possible varying mechanisms underlying surface UHI effect across spatial scales.

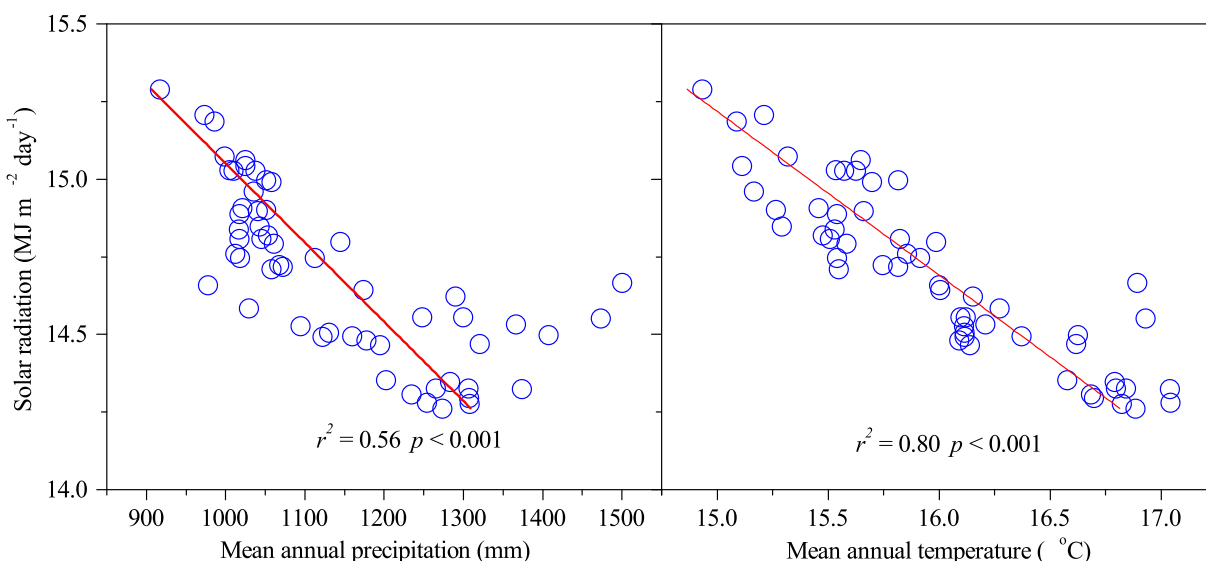


Fig. 12. Relationship between solar radiation and mean annual precipitation or air temperature across cities ($N = 56$).

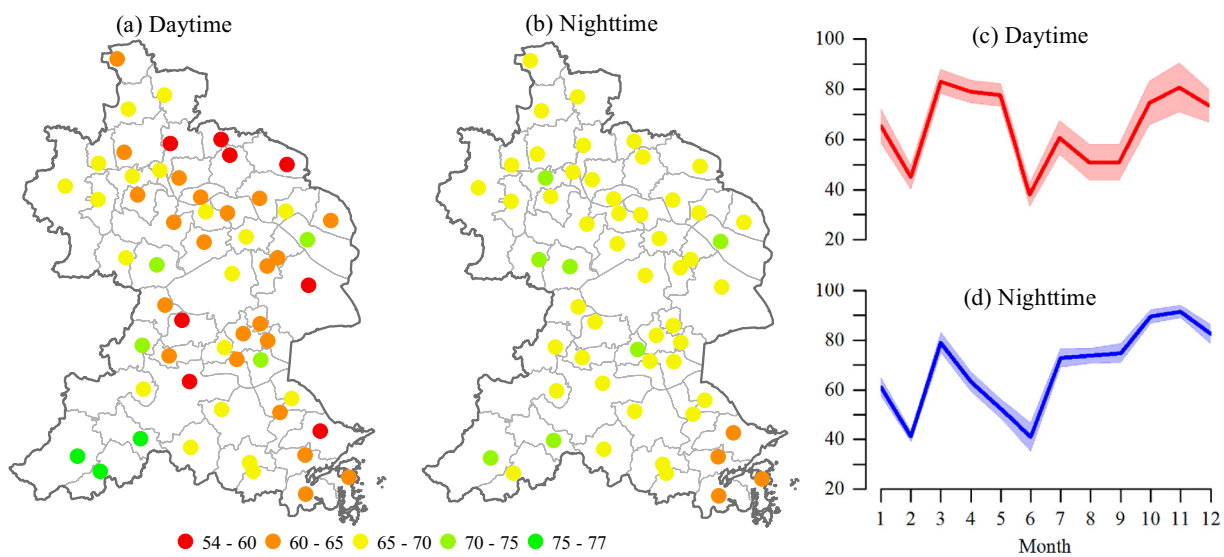


Fig. 13. Percentage of the date with valid SUHII estimation from 8-days MODIS LST products (a, b) and its mean monthly distribution (the shaded area represents one standard deviation across cities) (c, d).

4.2. Seasonal variability of SUHII in YRDUA and their drivers

This study demonstrated great seasonal changes of SUHII in YRDUA as characterized by overall larger intensity in summer than in winter (Fig. 6), which was highly consistent with the previous reports (Du et al., 2016; Imhoff et al., 2010; Peng et al., 2012; Zhou et al., 2014b). Difference in thermal admittance (which determines the warming and cooling rate) between urban and rural areas was mainly responsible for the seasonality (B. Zhou et al., 2015). In the forest area, the thermal admittance is highly subject to soil moisture and vegetation, and thus exhibit pronounced seasonal variations of the warming and cooling rates. As a result, the SUHII peaked in summer (Figs. 6 and 7) when urban warming rate and forest evaporative cooling effects reach their maximum. This mechanism can be proved by the strong positive relationships of precipitation, temperature, and solar radiation, and negative relationship of vegetation activity with SUHII across months (Fig. 11). Similar to the spatial pattern (Fig. 10), wind speed and surface albedo contributed little to the SUHII's seasonal trends (Fig. 11).

Note that other factors such as the anthropogenic heat flux and shading effects of buildings may also play important roles. For instance, heat releases caused by the extensive air conditioning usage in summer can exaggerate the SUHII (Wang et al., 2016). Meanwhile, tall buildings can easily form shadows in the YRDUA due to the low solar altitude in winter, and thus decrease the LST in urban areas (Du et al., 2016).

Particularly, cold island effect has been observed in YRDUA in winter for about one-third of cities during the day and the majority of cities at night. A possible reason is the combined effect of the heavy air pollution and the low vegetation activity in winter (Zhou et al., 2014b). The former reduced urban temperature by decreasing incoming solar radiation, and the latter exerted little cooling effects on rural surface, especially at night (Li and Bou-Zeid, 2013).

4.3. Implications and uncertainties

Urban agglomeration has become one of the most salient features of recent urbanization worldwide (Wu, 2014). This study investigated the SUHII distribution in one of the most densely populated urban agglomerations over the world. The results arrived in this paper might help enhance our understanding of surface UHI effect both regionally and globally. Our results showed that there were significant surface UHI effects in spite of urban area size (the largest SUHII in fact do not happen

in the core city), stressing the importance of considering cities altogether when making decisions about future of urban environments in an urban agglomeration region. In addition, we confirmed that the widely used urban-rural/suburban difference method was not appropriate for estimating SUHII in urban agglomerations, especially for the core cities, calling for efforts to reevaluate the SUHII's distribution of large cities. The quantitative method used from this study might provide new insights for such future efforts. Further, this study emphasized the importance of vegetation, urban area size, population density, and surface albedo in mitigating UHI effects as advocated by many previous studies, but the mitigation potential is limited during the daytime due to the strong control of background climate.

Uncertainties remained in this study. First, there may be certain biases in the fitted reference LST in the northeastern parts of the study region due to the lacking of natural forest pixels in such area (Fig. 3b). For example, proximity to ocean will induce land sea breeze circulations that have a moderating influence on the UHI (Vahmani and Ban-Weiss, 2016). This can be exemplified by the slight overestimation of daytime SUHII and underestimation of nighttime SUHII by method 2 which ignored the longitudinal effects (Fig. 9a and b). Fortunately, the SUHII's distributions estimated by method 2 were similar to that by method 1, suggesting a relatively small contribution of land sea breeze to SUHII as compared to other land surface properties in the study area. Second, the data qualities always act as a major source for the uncertainties. Taking the 8-days MODIS LST data products as an example, the data were invalid in over 30% of the total time periods after the data quality control, especially in February and June (Fig. 13). This may be mainly responsible for the weak nighttime SUHII in June (Fig. 7) and at least partially contributes to the seasonal variations of the correlations between SUHII and driving factors (Fig. 10). Third, this study examined the SUHII for clear days, the intensity of which might be significantly larger than that in cloudy days (B. Zhou et al., 2015). This implied that the actual annual mean SUHII might be lower than that estimated in this analysis if taking cloudy days into account. How to detect LST in cloudy conditions remains a grand challenge in remote sensing techniques (Jin and Dickinson, 2010). Fourth, some relationships between SUHII and potential drivers revealed in this study were contrary to previous findings, and the reasons remain elusive. For example, this study showed a significant effect of vegetation activity on nighttime SUHII (Fig. 10), contrary to the insignificant effects as reported in previous works (Peng et al., 2012; Zhou et al., 2014b). Finally, a more complete understanding of SUHII's variations needs the investigation of other

factors not analyzed here such as landscape configuration (Li et al., 2011; W. Zhou et al., 2017), the presence of water bodies, land use and atmospheric environment (Oke, 1982).

5. Conclusions

This study focused on the surface UHI effects in all the cities or city-administered counties of a highly developed urban agglomeration in eastern China. Since urban agglomeration has become a global trend, this research provides important insights on evaluating surface UHI effect in future cities and thus the related consequences. Our results showed that ignoring urban agglomeration effect (taking loosely defined suburban/rural area as unaffected reference) would underestimate SUHII substantially and even alter the distribution of SUHII estimates. Using natural forests as reference instead, this study indicated significant SUHII in YRDUA regardless of urban area size, with the magnitude clearly larger in the day than that at night. The SUHII varied markedly by cities that related closely to the background air temperature, precipitation, and vegetation activity in the day, and to population density, vegetation activity, and surface albedo at night. As a result, the strongest SUHII didn't happen in the presumed core cities (Shanghai, Nanjing, and Hangzhou) that possess relatively larger urban areas. Also, we found that the SUHII differed greatly by season that depend strongly on the background precipitation, air temperature, solar radiation, and vegetation activity during both the day and night. These results stress the necessity of considering cities altogether when making decisions about the future of urban environments in an urban agglomeration area, and call for efforts to revisit the SUHII of global big cities. However, uncertainties remained in current research, more in-depth comparison studies in combination with attribution analyses and numeric modeling are needed to verify the findings from present study.

Acknowledgements

This study was supported by the National Natural Science Foundation of China (#41501465, #41601196, and #31570464), and the Startup Foundation for Introducing Talent of NUIST (2014r051).

References

- Amiballe, R., Bonafoni, S., Pichieri, M., 2014. Spatial and temporal trends of the surface and air heat island over Milan using MODIS data. *Remote Sens. Environ.* 150, 163–171.
- Arnfield, A.J., 2003. Two decades of urban climate research: a review of turbulence, exchanges of energy and water, and the urban heat island. *Int. J. Climatol.* 23, 1–26.
- Chen, J., Jönsson, P., Tamura, M., Gu, Z., Matsushita, B., Eklundh, L., 2004. A simple method for reconstructing a high-quality NDVI time-series data set based on the Savitzky-Golay filter. *Remote Sens. Environ.* 91, 332–344.
- CIESIN. Center for International Earth Science Information Network of Columbia University, 2016. Documentation for the Gridded Population of the World, Version 4 (GPWv4). NASA Socioeconomic Data and Applications Center (SEDAC), Palisades NY.
- Clinton, N., Gong, P., 2013. MODIS detected surface urban heat islands and sinks: global locations and controls. *Remote Sens. Environ.* 134, 294–304.
- Du, H., Wang, D., Wang, Y., Zhao, X., Fei, Q., Hong, J., et al., 2016. Influences of land cover types, meteorological conditions, anthropogenic heat and urban area on surface urban heat island in the Yangtze River Delta Urban Agglomeration. *Sci. Total Environ.* 571, 461.
- Fang, C., 2015. Important progress and future direction of studies on China's urban agglomerations. *J. Geogr. Sci.* 25, 1003–1024.
- Fick, S.E., Hijmans, R.J., 2017. WorldClim 2: new 1-km spatial resolution climate surfaces for global land areas. *Int. J. Climatol.* 37, 4302–4315.
- Grimm, N.B., Faeth, S.H., Golubiewski, N.E., Redman, C.L., Wu, J., Bai, X., et al., 2008. Global change and the ecology of cities. *Science* 319, 756–760.
- Hall, A., 2004. The role of surface albedo feedback in climate. *J. Clim.* 17, 1550–1568.
- Hao, L., Sun, G., Liu, Y., Wan, J., Qin, M., Qian, H., et al., 2015. Urbanization dramatically altered the water balances of a paddy field dominated basin in Southern China. *Hydrol. Earth Syst. Sci.* 19, 3319–3331.
- Howard, L., 1833. Climate of London Deduced from Metrological Observations. vol. 1. Harvey and Dorton Press, London.
- Huang, Q., Lu, Y., 2015. The effect of urban heat island on climate warming in the Yangtze River Delta urban agglomeration in China. *Int. J. Environ. Res. Public Health* 12, 8773–8789.
- Imhoff, M.L., Zhang, P., Wolfe, R.E., Bounoua, L., 2010. Remote sensing of the urban heat island effect across biomes in the continental USA. *Remote Sens. Environ.* 114, 504–513.
- Jin, M.L., Dickinson, R.E., 2010. Land surface skin temperature climatology: benefitting from the strengths of satellite observations. *Environ. Res. Lett.* 5, 044004.
- Kong, F., Yin, H., James, P., Hutyra, L.R., He, H.S., 2014. Effects of spatial pattern of greenspace on urban cooling in a large metropolitan area of eastern China. *Landscape Urban Plan.* 128, 35–47.
- Kruse, F.A., Lefkoff, A.B., Boardman, J.W., Heidebrecht, K.B., Shapiro, A.T., Barloon, P.J., et al., 1993. The Spectral Image Processing System (SIPS)—interactive visualization and analysis of imaging spectrometer data. *Remote Sens. Environ.* 283, 145–163.
- Li, D., Bou-Zeid, E., 2013. Synergistic interactions between urban heat islands and heat waves: the impact in cities is larger than the sum of its parts. *J. Appl. Meteorol. Climatol.* 52, 2051–2064.
- Li, J., Song, C., Cao, L., Zhu, F., Meng, X., Wu, J., 2011. Impacts of landscape structure on surface urban heat islands: a case study of Shanghai, China. *Remote Sens. Environ.* 115, 3249–3263.
- Li, Y., Zhang, H., Kainz, W., 2012. Monitoring patterns of urban heat islands of the fast-growing Shanghai metropolis, China: using time-series of Landsat TM/ETM + data. *Int. J. Appl. Earth Obs. Geoinf.* 19, 127–138.
- Li, W., Bai, Y., Chen, Q., He, K., Ji, X., Han, C., 2014. Discrepant impacts of land use and land cover on urban heat islands: a case study of Shanghai, China. *Ecol. Indic.* 171–178.
- Li, X., Zhou, Y., Asrar, G.R., Imhoff, M., Li, X., 2017. The surface urban heat island response to urban expansion: a panel analysis for the conterminous United States. *Sci. Total Environ.* 605–606, 426.
- Li, H., Zhou, Y., Li, X., Meng, L., Wang, X., Wu, S., et al., 2018. A new method to quantify surface urban heat island intensity. *Sci. Total Environ.* 624, 262–272.
- Oke, T.R., 1973. City size and the urban heat island. *Atmos. Environ.* 7, 769–779.
- Oke, T.R., 1982. The energetic basis of the urban heat island. *Q. J. R. Meteorol. Soc.* 108, 1–24.
- Patz, J.A., Campbell-Lendrum, D., Holloway, T., Foley, J.A., 2005. Impact of regional climate change on human health. *Nature* 438, 310–317.
- Peng, S., Piao, S., Ciais, P., Friedlingstein, P., Ottle, C., Bréon, F.M., et al., 2012. Surface urban heat island across 419 global big cities. *Environ. Sci. Technol.* 46, 696–703.
- Peng, J., Xie, P., Liu, Y., Ma, J., 2016. Urban thermal environment dynamics and associated landscape pattern factors: a case study in the Beijing metropolitan region. *Remote Sens. Environ.* 173, 145–155.
- Peterson, T.C., 2003. Assessment of urban versus rural in situ surface temperatures in the contiguous United States: no difference found. *J. Clim.* 16, 2941–2959.
- Santamouris, M., 2015. Analyzing the heat island magnitude and characteristics in one hundred Asian and Australian cities and regions. *Sci. Total Environ.* 512–513, 582–598.
- Santamouris, M., Asimakopoulos, D.D.N., 2001. Energy and Climate in the Urban Built Environment. Routledge.
- Santamouris, M., Cartalis, C., Synnefa, A., Kolokotsa, D., 2015. On the impact of urban heat island and global warming on the power demand and electricity consumption of buildings—a review. *Energ. Buildings* 98, 119–124.
- Schneider, A., 2009. A new map of global urban extent from MODIS satellite data. *Environ. Res. Lett.* 4, 44003–44011.
- Seto, K.C., Güneralp, B., Hutyra, L.R., 2012. Global forecasts of urban expansion to 2030 and direct impacts on biodiversity and carbon pools. *Proc. Natl. Acad. Sci. U. S. A.* 109, 16083–16088.
- Shepherd, J.M., 2005. A review of current investigations of urban-induced rainfall and recommendations for the future. *Earth Interact.* 9, 1–27.
- Shimada, M., Itoh, T., Motooka, T., Watanabe, M., Shiraiishi, T., Thapa, R., et al., 2014. New global forest/non-forest maps from ALOS PALSAR data (2007–2010). *Remote Sens. Environ.* 155, 13–31.
- Tachikawa, T., Hato, M., Kaku, M., Iwasaki, A., 2011. Characteristics of ASTER GDEM version 2, 2011 IEEE International Geoscience and Remote Sensing Symposium. pp. 3657–3660.
- UN. United Nations Department of Economic Social Affairs Population Division, 2015. *World Urbanization Prospects: The 2014 revision*. United Nations, New York.
- Vahmani, P., Ban-Weiss, G.A., 2016. Impact of remotely sensed albedo and vegetation fraction on simulation of urban climate in WRF-urban canopy model: a case study of the urban heat island in Los Angeles. *J. Geophys. Res.-Atmos.* 121, 1511–1531.
- Voogt, J.A., Oke, T.R., 2003. Thermal remote sensing of urban climates. *Remote Sens. Environ.* 86, 370–384.
- Wan, Z., 2014. New refinements and validation of the collection-6 MODIS land-surface temperature/emissivity product. *Remote Sens. Environ.* 140, 36–45.
- Wang, X., Sun, X., Tang, J., Yang, X., 2016. Urbanization-induced regional warming in Yangtze River Delta: potential role of anthropogenic heat release. *Int. J. Climatol.* 35, 4417–4430.
- Wang, K., Jiang, S., Wang, J., Zhou, C., Wang, X., Lee, X., 2017. Comparing the diurnal and seasonal variabilities of atmospheric and surface urban heat islands based on the Beijing urban meteorological network. *J. Geophys. Res.-Atmos.* 122, 2131–2154.
- Ward, K., Lauf, S., Kleinschmit, B., Endlicher, W., 2016. Heat waves and urban heat islands in Europe: a review of relevant drivers. *Sci. Total Environ.* 569–570, 527–539.
- Wu, J., 2014. Urban ecology and sustainability: the state-of-the-science and future directions. *Landscape Urban Plan.* 125, 209–221.
- Xu, M., He, C., Liu, Z., Dou, Y., 2016. How did urban land expand in China between 1992 and 2015? A multi-scale landscape analysis. *PLoS One* 11, e0154839.
- Yang, X., Hou, Y., Chen, B., 2011. Observed surface warming induced by urbanization in east China. *J. Geophys. Res.-Atmos.* 116, 263–294.

- Yang, X., Leung, L.R., Zhao, N., Zhao, C., Qian, Y., Hu, K., et al., 2017. Contribution of urbanization to the increase of extreme heat events in an urban agglomeration in east China. *Geophys. Res. Lett.* 6940–6950.
- Yonezawa, C., 2007. Maximum likelihood classification combined with spectral angle mapper algorithm for high resolution satellite imagery. *Int. J. Remote Sens.* 28 (16), 3729–3737.
- Zhao, L., Lee, X., Smith, R.B., Oleson, K., 2014. Strong contributions of local background climate to urban heat islands. *Nature* 511, 216–219.
- Zhou, D., Zhao, S., Liu, S., Zhang, L., 2014a. Spatiotemporal trends of terrestrial vegetation activity along the urban development intensity gradient in China's 32 major cities. *Sci. Total Environ.* 488, 136–145.
- Zhou, D., Zhao, S., Liu, S., Zhang, L., Zhu, C., 2014b. Surface urban heat island in China's 32 major cities: spatial patterns and drivers. *Remote Sens. Environ.* 152, 51–61.
- Zhou, B., Lauwaet, D., Hooyberghs, H., De Ridder, K., Kropp, J.P., Rybski, D., 2015. Assessing seasonality in the surface urban heat island of London. *J. Appl. Meteorol. Climatol.* 55, 151103140058003.
- Zhou, D., Zhao, S., Zhang, L., Sun, G., Liu, Y., 2015. The footprint of urban heat island effect in China. *Sci. Rep.* 5, 11160.
- Zhou, D., Li, D., Sun, G., Zhang, L., Liu, Y., Hao, L., 2016a. Contrasting effects of urbanization and agriculture on surface temperature in eastern China. *J. Geophys. Res.-Atmos.* 121, 9597–9606.
- Zhou, D., Zhang, L., Li, D., Huang, D., Zhu, C., 2016b. Climate–vegetation control on the diurnal and seasonal variations of surface urban heat islands in China. *Environ. Res. Lett.* 11, 074009.
- Zhou, D., Zhao, S., Zhang, L., Liu, S., 2016c. Remotely sensed assessment of urbanization effects on vegetation phenology in China's 32 major cities. *Remote Sens. Environ.* 176, 272–281.
- Zhou, B., Rybski, D., Kropp, J.P., 2017. The role of city size and urban form in the surface urban heat island. *Sci. Rep.* 7, 4791.
- Zhou, W., Wang, J., Cadenasso, M.L., 2017. Effects of the spatial configuration of trees on urban heat mitigation: a comparative study. *Remote Sens. Environ.* 195, 1–12.